Comparative Study of Deconvolution Algorithms for GPR Bridge Deck Imaging

I. ABDEL-QADER[1], V. KRAUSE[1], F. ABU-AMARA[2*], O. ABUDAYYEH[3]
[1]Department of Electrical and Computer Engineering
Western Michigan University
1903 W. Michigan Ave., Kalamazoo, MI 49008-5329
USA
ikhlas.abdelqader@wmich.edu, vincent.a.krause@wmich.edu

[2]Department of Computer Engineering
Al-Hussein Bin Talal University
P.O.Box: 104, Ma□an
Jordan
fadiabuamara@ahu.edu.jo

[3]Department of Civil and Construction Engineering
Western Michigan University
1903 W. Michigan Ave., Kalamazoo, MI 49008-5329
USA
osama.abudayyeh@wmich.edu

Abstract: - Bridge decks deteriorate over time as a result of freezing-and-thawing, heavy use, and water penetration resulting in internal defects. Ground penetrating radar (GPR) can be used as a non-destructive method for detecting such defects. Unfortunately, reflections from closely spaced objects overlap which prevents the accurate estimation of the round-trip travel time of GPR waves to the closely spaced objects. In this paper, singular value decomposition (SVD), subset selection (SSDA), and independent component analysis (ICA) deconvolution algorithms are used to solve this problem using GPR scans of simulated concrete bridge decks. Then, velocity analysis method is used to estimate depth of defects as an evaluation criterion. Results show that ICA has better performance than SVD and SSDA at a cost of slower execution time.

Key-Words: - Singular value decomposition, subset selection deconvolution algorithm, independent component analysis, ground penetrating radar, bridge condition assessment, non-destructive testing

1 Introduction

Bridge and road structures consist of layers of concrete, soil, asphalt, and rebar. These structures deteriorate over time as a result of freezing-and-thawing, heavy use, water penetration, and deicing salts, leading to internal defects. Ground penetrating radar (GPR) can be used to detect defects such as delaminations and air-filled voids inside concrete structures such as in bridge decks and roads [1-2]. Delaminations result from rebar corrosion due to moisture and deicing salts which causes a fracture plane to develop, resulting in the creation of concrete-air-concrete interfaces in raw GPR scans.

However, the analysis of GPR scans is typically done manually and may lead to errors in interpretation. Also, the manual processing of GPR scans is time-consuming. Therefore, the motivation behind the work discussed in this paper is to find automated and accurate signal analysis techniques for processing GPR scans to eliminate human interpretation errors and reduce the condition assessment time.

The most commonly used non-destructive testing formats for GPR data presentation are known by the A-scans and B-scans. The A-scan is conducted at a single location where raw GPR data are represented as a column vector (a trace). The B-scan is conducted by moving a GPR antenna over the target surface and then recording the reflected signals at regular intervals. An example of a B-scan is shown in Fig. 1. Each column of the B-scan is a single A-scan taken at the x^{th} location.

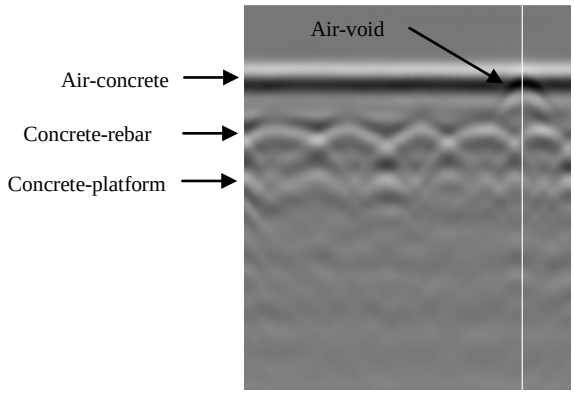

Fig.1: A raw GPR scan data from a 15-cm slab with embedded air-void defect

Once the transmitted radar pulse hits the target, it is reflected and refracted at every boundary between any two electrically different materials that it passes through. Fig. 1 shows an actual GPR scan taken from a 15-cm slab of concrete with embedded air-void defect. Using the standard model of interpreting GPR scans, the horizontal bands at the top of the image represent air-concrete interface. The hyperbolic arcs represent the concrete-rebar interface [3]. We expect to see horizontal lines representing reflections from the concrete-to-slab bottom interface. These reflections show non-continuous segments because they destructively interfere with reflections from the distant rebar. As Fig. 1 shows, there is interference between the hyperbolic tails causing spurious hyperbolic arcs which may obscure reflections from underneath targets. The migration method can be used to eliminate such artifacts [3]. In the case of bridge deck condition assessment, the medium is known and the deterioration, which is usually formed around the rebar mesh, is not masked by these artificial hyperbolae. Fig. 2 shows an extracted trace at column 255 from the B-scan of Fig. 1 where the three above interfaces are marked as 1, 2, and 3. The reflected GPR signals from closely spaced objects overlap. Therefore, reflections from the shallow air-void defect are completely overlapped with reflections from air-concrete interface. Also, a partial overlapping is shown between reflections from concrete-rebar and concrete-platform interfaces.

Deconvolution can be used to reduce the overlapping and improve the estimation accuracy of the round-trip travel time of GPR waves to the closely spaced objects. Deconvolution transforms the broad reflected pulses in GPR scan data into "sharp" spikes. Many algorithms are proposed and used for deconvolution such as Fourier-based algorithms [4], Optimization-based algorithms [5], blind deconvolution algorithms [6-7], discrete wavelet transform based algorithms [8], correlation-based methods [9], and conjugate gradient methods [10] to list few.

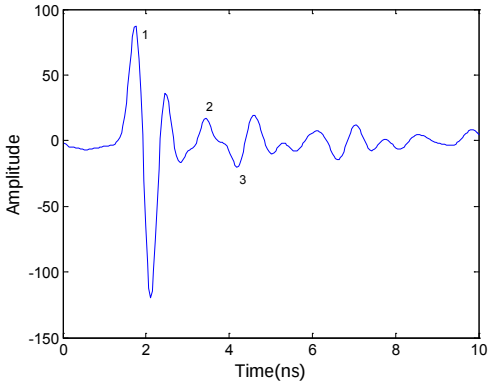

Fig.2: An extracted trace at column 255 (marked by white vertical line in Fig. 1)

Six different deconvolution methods were examined including Wiener-based methods using GPR data [11]. It was reported that the Homomorphic deconvolution outperformed all the other methods they considered. Also, a comparison between Weiner deconvolution, Homomorphic deconvolution, singular value decomposition (SVD), subset selection deconvolution algorithm (SSDA), and Discrete wavelet transform was conducted for deconvolving GPR data [12]. They reported that SVD outperformed the other algorithms where the values of the amplitude of the embedded targets and their depth in the recovered impulse response of the scanned medium using SVD were closer to the actual measurements in comparison with results of the other algorithms.

The ultimate goal of our project is to automate the process of analyzing GPR scans using techniques that detect and identify defects in concrete bridge decks. The work presented in this paper focuses on investigating direct and blind deconvolution algorithms to achieve our goals. Three techniques are chosen for the comparative study: 1) the singular value decomposition (SVD) is selected as a classical tool for direct deconvolution, 2) the subset selection deconvolution algorithm (SSDA) is selected as another direct deconvolution technique that is intrinsically different from SVD as SVD is not a transform based algorithm while SSDA is, and 3) the independent component analysis (ICA) is selected because it is a recent technique for blind signal separation.

2 Background on Deconvolution Algorithms

Raw GPR data are complex and difficult to analyze because it is a convolutive mixture of the transmitted signal (incident pulse) and the reflective characteristics of the target slab (impulse response of the slab). Deconvolution is sought in this work as a preprocessing step for the automation of embedded defects' detection and identification. The measured response g and the incident pulse f are related by

$$g = f * h = \sum_j f(t_{i-j})h(t_j) \tag{1}$$

where * represents the mathematical convolution operation and h represents the impulse response of the system (i.e., what characterizes the scanned slab, its internal objects and defects, and the measurement system). The incident pulse of the 1.5 GHz (GSSI model 5100) bistatic antenna is estimated by transmitting a pulse into a metal plate (a perfect reflector) and recording the reflected signal as shown in Fig. 3 [9]. The convolution process can be modeled using matrix operations as shown in Equations 2 and 3 where columns of the convolution matrix F are constructed from delayed versions of the incident pulse vector $f = [f(t_1), f(t_2), \cdots, f(t_{nw})]^T$.

$$g = Fh \tag{2}$$

$$F_{n\times n} = \begin{bmatrix} f(t_1) & 0 & 0 & 0 & 0 & 0 \\ \vdots & f(t_1) & 0 & 0 & 0 & 0 \\ f(t_{nw}) & \vdots & \ddots & \vdots & \vdots & \vdots \\ 0 & f(t_{nw}) & & f(t_1) & 0 & \\ \vdots & 0 & \ddots & \vdots & & 0 \\ 0 & 0 & & f(t_{nw}) & f(t_{nw-1}) \cdots & f(t_1) \end{bmatrix} \tag{3}$$

where n is the number of samples of the GPR trace g, nw is the number of samples of the discrete random vector f, t_i represents time index, and $i = 1, 2, \cdots, nw$. Typically F will be a large matrix with near zero main diagonal values and so it is an ill-conditioned matrix that may not have an inverse. If an inverse does exist, F^{-1} may be extremely sensitive to additive noise in g and consequently, h may not be easily estimated.

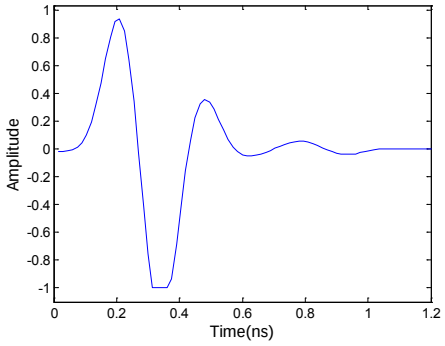

Fig.3: The estimated incident pulse of the 1.5 GHz antenna

3 Framework and Modeling

3.1 Singular Value Decomposition (SVD)

In general, singular value decomposition (SVD) is used to decompose a real or complex matrix F as the product of an $M \times M$ column-orthogonal matrix U, an $M \times N$ diagonal matrix Σ, and an $N \times N$ column-orthogonal matrix V [13]. Using SVD method, the convolution matrix F can be decomposed using Equation (4),

$$F = U\Sigma V^T \tag{4}$$

where Σ is a diagonal matrix whose entries are the singular values (i.e., the absolute values of the eigenvalues) on the diagonal direction. SVD transforms the original matrix into a domain where the covariance matrix is diagonal with singular values given by

$$\sum_{ii} = \sigma_i \quad and \quad \sigma_i \geq \sigma_{i+1}$$

Using SVD, the convolution in Equation (1) may be restated as

$$g = \sum_i (v_i^T \cdot h)\sigma_i u_i \tag{5}$$

and thus an inverse process can be constructed using matrix operations resulting in an estimate of the impulse response h

$$h = \sum_i \frac{(u_i^T \cdot g)v_i}{\sigma_i} \tag{6}$$

For several reasons, this inversion tends to fail. Some σ_i may equal to zero making the division process impossible. Some σ_i may be smaller than

machine precision resulting in machine errors in division. Additionally, additive noise in *g* may be greatly amplified if it correlates to unit vectors with a small σ_i. One solution is to replace the division by σ_i with multiplication by a similar yet better-behaved function. The approach can be described as

$$h = \sum_i (u_i{}^T . g)\, p(\sigma_i)\, v_i \tag{7}$$

where

$$p(\sigma_i) = \begin{cases} \dfrac{1}{\sigma_i} & when \quad \sigma_i \geq threshold \\ 0 & when \quad \sigma_i < threshold \end{cases}$$

The choice of threshold allows us to avoid division errors and to discard components of *g* which are determined to be mostly noise. To deconvolve an A-scan of GPR data using SVD method, a convolution matrix *F* is created based on the transmitted pulse *f* as modeled in Equation (3). Matrix *F* is then decomposed into its *U*, Σ and *V* components, and a threshold for values of σ_i is chosen. Equation (7) is then used to process the corresponding GPR trace *g*. The resulting *h* vector should show signature of the embedded objects and possible defects.

3.2 Subset Selection Deconvolution Algorithm (SSDA)

SSDA assumes that the real data *g* can be closely approximated by convolving the transmitted pulse *f* with a small number of delta function pulses [9,14]. The time delays and amplitudes of these delta functions are chosen to minimize Equation (8), similar to the linear least squares method,

$$\min_{\tau_i, a_i} \left[\left\| \left(\sum_i a_i \delta(t - \tau_i) \right) * f - g \right\|_2^2 \right] \tag{8}$$

where a_i and τ_i represent amplitude and delay time of the corresponding impulse function. Finding the values of τ_i and a_i which minimize Equation (8) is a non-trivial challenge especially for large values of *i*. When a minimum is found, the sought impulse response of the medium is

$$h = \left(\sum_i a_i \delta(t - \tau_i) \right) \tag{9}$$

If the difference in delay times of two separate pulses is under a preselected critical threshold value ($T = 0.214ns$), SSDA will detect a single pulse whose delay time is roughly the average of the two original pulses and whose amplitude is their sum. Such a false detection obscures the true position of pulses, and generates noise which may obscure low amplitude details. The success of SSDA relies on the initial choices of τ_i and a_i. To deconvolve a GPR trace *g* using SSDA, the number of expected pulses *i* is selected and the minimum values of τ_i and a_i are found using the Gauss-Newton's optimization method which is an iterative-based method and then the vector *h* is reconstructed using Equation (9).

3.3 Independent Component Analysis (ICA)

Independent component analysis (ICA) is a statistical technique that can be used to solve problems in blind signal separation as it has the ability to blindly decompose hidden components within a set of observed data [15]. The discrete convolution model of Equation (1) can be expressed as a linear ICA model ($x = As$) where the radar trace vector is defined as $x = [g(t_1), g(t_2), \cdots, g(t_n)]^T$, the impulse response vector is defined as $s = [h(t_1), h(t_2), \cdots, h(t_n)]^T$, and the mixing matrix *A* is defined according to Equation (3). As Equation (3) indicates, the mixing matrix *A* is a banded matrix with the nonzero elements of its columns contain the unknown incident pulse vector. This prior information can be utilized to convert a blind deconvolution problem into a blind source separation problem [16]. However, this represents a single-input single-output instantaneous ICA model which is inadequate since statistics of the independent components cannot be characterized. In order to form a multiple-input multiple-output ICA model ($X = AS$), time delayed versions of *x(t)* and *s(t)* are used to construct multidimensional matrices as shown in the following equations [15].

$$X_{m \times n} = [x(t-m+1)\ x(t-m+2)\ \cdots\ x(t-1)\ x(t)]^T \tag{10}$$

$$S_{m \times n} = [s(t-m+1)\ s(t-m+2)\ \cdots\ s(t-1)\ s(t)]^T \tag{11}$$

where m < n. Let *g* represent an A-scan, the proposed banded-ICA algorithm can be summarized in the following steps:

- The trace is centered to make its mean zero.
- The mixture matrix *X* is constructed according to Equation (10).

- The matrix X is whitened using the Mahalanobis transformation according to the following Equation [17].

$$Z = C^{-0.5}(X - \overline{X}) \quad (12)$$

where C is the covariance matrix and $\overline{X}$ is the mean of the matrix X. The whitening process uncorrelates components of a centered vector and results in unity variances and identity covariance matrix.

- A statistical efficient version of the FastICA algorithm (EFICA) is used to obtain the estimated independent components [18]. EFICA is a slightly higher computationally demanding than FastICA algorithm [19] but has superior separation performance.
- ICA recovers a number of independent components equal to m. The source signal that needs to be estimated (impulse response of the concrete slab) is a sparse signal representing the layered structure of the scanned concrete slab. It consists of a number of sharp spikes with relatively flat area between them. Therefore, the independent component with a number of spikes according to Equation (13) and with the highest sparsity is selected as the best candidate. Equation 14 has been used to measure sparsity of a signal since Y would be higher in magnitude when the signal is more sparse [20].

$$N_{\max} \in [N_s - 1, N_s + 1] \quad (13)$$

where N_s represents number of interfaces in the scanned concrete slab. The defect sometimes masks reflections from objects underneath it (rebar and concrete-platform interfaces) while it adds extra interface other times.

$$Y = \frac{\sqrt{\frac{1}{N}\sum_{i=1}^{N} y^2(i)}}{\frac{1}{N}\sum_{i=1}^{N} |y(i)|} = \sqrt{N}\,\frac{\sqrt{\sum_{i=1}^{N} y^2(i)}}{\sum_{i=1}^{N} |y(i)|} \quad (14)$$

4 Velocity-Analysis Based Depth Estimation and Experimental Results

The previous deconvolution algorithms estimate the round-trip travel time of GPR waves to the detected defects. In order to evaluate their performance, velocity-analysis method is used to estimate depth from the round-trip travel time and compare it with the actual depth. It can be summarized in the following steps:

1. Velocity of GPR waves through the medium can be estimated per Equation (15).

$$V = \frac{2d_r}{t_r} \quad (15)$$

where V is the speed in m/s, d_r is rebar depth, and t_r is the round-trip travel time to the rebar.

2. The actual depth of the defect is found using Equation (16). The round-trip travel time of the defect t_t and rebar are found from the deconvolved trace which contains spikes correspond to ground line, defect, rebar, and substrate interfaces.

$$d_t = \frac{t_t V}{2} \quad (16)$$

In this work, we used two types of GPR scans, synthetic and real scans. In the following subsections we present analysis using two synthetic traces and nine real GPR traces.

4.1 Results Using Synthetic GPR Scans

By convolving the incident pulse of Fig. 3 with the synthetic impulse responses of Fig. 4, synthetic traces are obtained as shown in Fig. 5. The two impulse responses of Fig. 4 model a concrete slab with three layers, ground line, rebar, and substrate. The arrival times of Fig. 4(A) are 0.3ns, 2.085ns, and 2.385ns resulting in differential time delays of $\Delta t_1 = 1.785\,ns$ and $\Delta t_2 = 0.3\,ns$ while Fig. 4(B) indicates arrival times of 0.3ns, 2.205ns, and 2.25ns with differential times of $\Delta t_1 = 1.905\,ns$ and $\Delta t_2 = 0.045\,ns$. Since bandwidth of the GSSI (Geophysical Survey Systems, Inc.) antenna is approximately equal to its center frequency [3], the incident pulse of Fig. 3 has duration of $T = 1/B = 1/1.6\,GHz = 0.625\,ns$. The overlapping between the second and third reflections of Fig. 5(A) is a result of the fact that their differential time delays (Δt) are less than duration of the incident pulse. The second and third reflections of Fig. 5(B) are completely overlapped while partial overlapping is shown in Fig. 5(A).

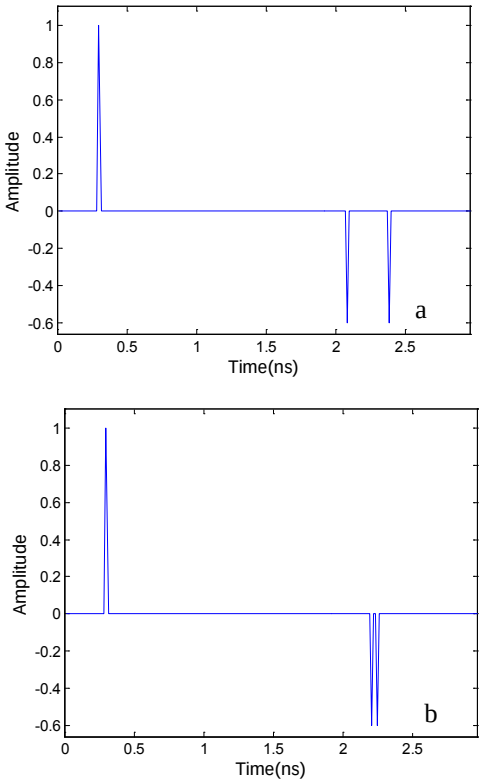

Fig.4: A and B are two synthetic impulse responses both consisting of three spikes

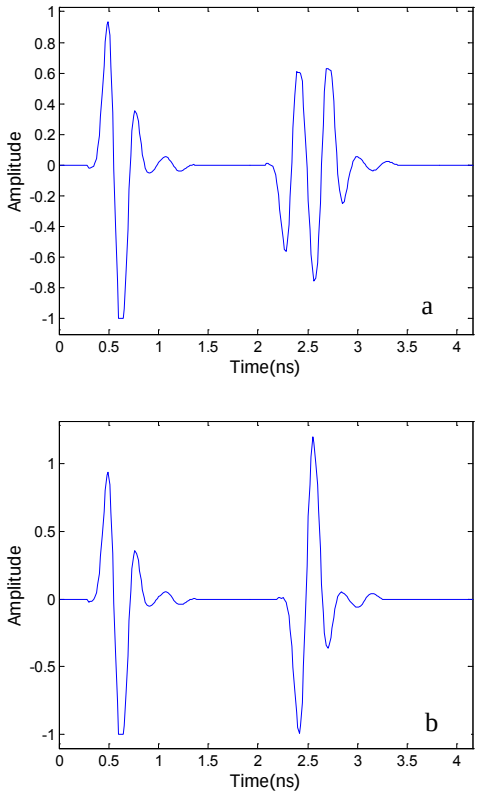

Fig.5: A and B are synthetic traces with overlapping second and third reflections

The process of determining the best threshold value for the singular values of Equation (7) should be automated. In a previous work, it was found that the reconstructed impulse response using number of singular values equal to the cut-off frequency of the power spectrum of the corresponding GPR trace can accurately represent the impulse response of the scanned medium [21]. This due to the fact that most information in the data are captured by few number of singular values. Using SVD algorithm, Fig. 6 shows the retrieved impulse responses of Fig. 4 scans with 137 singular values.

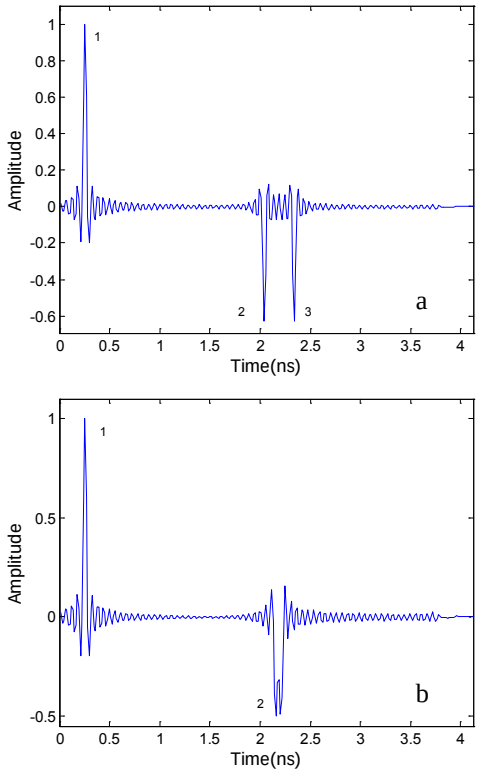

Fig.6: A and B are the retrieved impulse responses of figure 4 using SVD

Figs. 7 and 8 show the retrieved impulse responses of Fig. 4 using the SSDA and ICA algorithms. The estimated impulse responses using SSDA and ICA are sparse in comparison with results of SVD indicating their similarity to the original sparse impulse responses. Since the second and third spikes of Fig. 4(B) have a differential time delay less than the threshold for SVD and SSDA to detect, both detect a spike whose differential time delay is roughly the average of the two original spikes and whose amplitude is their sum as Figs. 6(B) and 7(B) show. In both results of SSDA and ICA, one can notice that spike amplitudes are inconsistent with original ones of Fig. 4 due to the scaling ambiguity of the optimization method used

in both SSDA and ICA algorithms. However, since the ultimate goal is to determine spike location which corresponds to target's depth, this is not a problem.

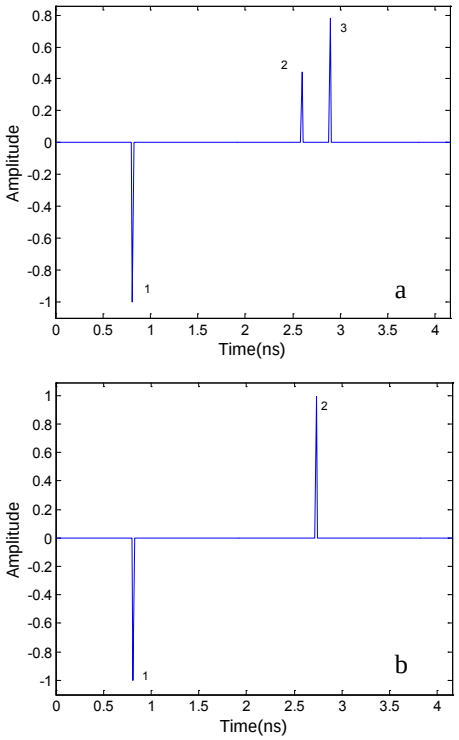

Fig.7: A and B are the retrieved impulse responses of figure 4 using SSDA

Table 1 shows the measured (Δt_m) and estimated (Δt_e) differential time delays between the largest three spikes of the estimated impulse response of Fig. 4(A) using the three methods. The differential time delay is chosen for the comparison between the methods since it shows location of the other spikes relative to the first spike and thus location of a target/defect can be determined relative to location of the first spike which represents the ground line. The best results are obtained using the SVD and ICA algorithms. On the other hand, Table 2 shows the actual and estimated differential time delays between the largest three spikes of the estimated impulse response of Fig. 4(B). As the table indicates, ICA algorithm is the only one able to detect the very small differential time delay between the second and third spikes. Results of Tables 1 and 2 indicate that ICA has better performance than SVD and SSDA.

4.2 Results Using Real GPR Scans

A simulated 114-cm long by 114-cm wide by 15-cm deep concrete bridge deck (slab) is constructed with embedded defects of known locations and dimensions with a bottom layer of rebar in both directions at depth of 6-cm and 7.6-cm. Air voids are simulated by embedding PVC (Polyvinyl Chloride) pipes of different lengths and diameters while delaminations are simulated by embedding Styrofoam blocks in the concrete that are later dissolved using acetone. Fig. 9 shows a slab with embedded defects. The simulated bridge deck was scanned using the GPR antenna described earlier in a ground coupled mode. The GPR antenna is set to 3.3 scans per cm during the data collection process. The determination of this number is based on the antenna frequency, estimated size of smallest target, and estimated depth of the shallowest target. Nine scans are performed and labeled scans 1 through 9 in order to test performance of the proposed deconvolution algorithms. These scans cover all the defects in the constructed concrete slab with different scanning directions and locations.

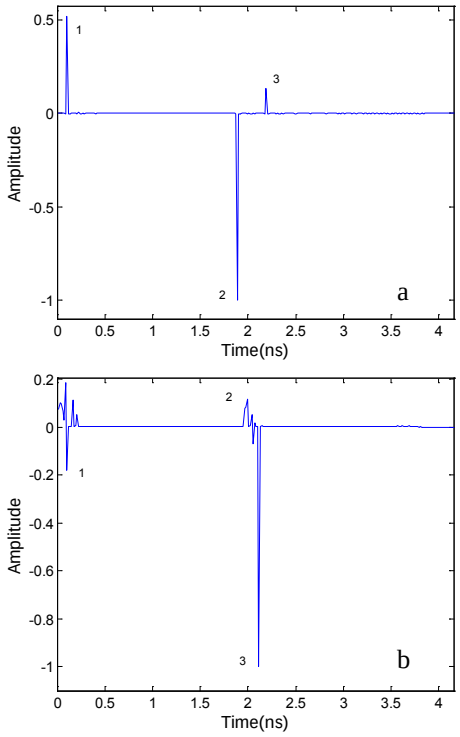

Fig.8: A and B are the retrieved impulse responses of figure 4 using ICA

Fig. 1 shows the GPR scan data (scan1) from the concrete slab with embedded rebar and air-void defect. The black section of the ground coupling band is obscured by the embedded defect as shown in the figure. Also, the fourth and fifth rebar arcs look brighter than other rebar arcs due to the embedded defect. Fig. 2 shows an extracted trace at column 255 representing a defective trace.

Fig. 10(A) shows a raw B-scan (scan2) with two embedded delamination defects. Fig. 10(B) and Fig.

10(C) show extracted traces at the center of the defective regions. The first defect masked reflections from underneath objects and overlapped with the ground coupling band as shown in Fig. 10(B) while the second defect was totally overlapped with rebar reflections as shown in Fig. 10(C). Fig. 11(A) shows a raw B-scan (scan3) with embedded air-void defect. Fig. 11(B) shows an extracted trace at the center of the defective region where the defect is overlapped with rebar reflections.

Table 1: Measured and estimated differential times of the first impulse response

Method	Δt	Δt_m (ns)	Δt_e (ns)	Diff (ns)
SVD	Δt_1	1.785	1.785	0
	Δt_2	0.3	0.3	0
SSDA	Δt_1	1.785	1.77	0.015
	Δt_2	0.3	0.3	0
ICA	Δt_1	1.785	1.785	0
	Δt_2	0.3	0.3	0

Table 2: Measured and estimated differential times of the second impulse response

Method	Δt	Δt_m (ns)	Δt_e (ns)	Diff (ns)
SVD	Δt_1	1.905	1.905	0
	Δt_2	0.045	0	0.045
SSDA	Δt_1	1.905	1.905	0
	Δt_2	0.045	0	0.045
ICA	Δt_1	1.905	1.905	0
	Δt_2	0.045	0.045	0

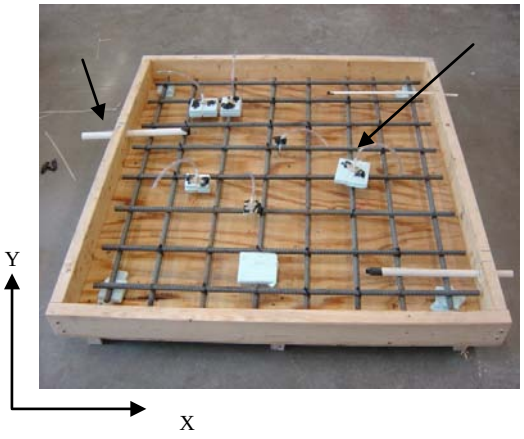

Fig.9: A laboratory concrete slab with embedded defects

Fig. 12(A) shows a raw B-scan (scan4) with embedded delamination and air-void defects. Fig. 12(B) shows overlapping with rebar reflections while Fig. 12(C) shows partial overlapping. Fig. 13(A) shows a raw B-scan (scan5) with embedded delamination and air-void defects. Fig. 13(B) and Fig. 13(C) show overlapping between defect and ground line reflections. In Fig. 13(B), the defect is barely visible due to the low contrast with its background. The rest of the scans and the scanning process are summarized in Tables 3 and 4.

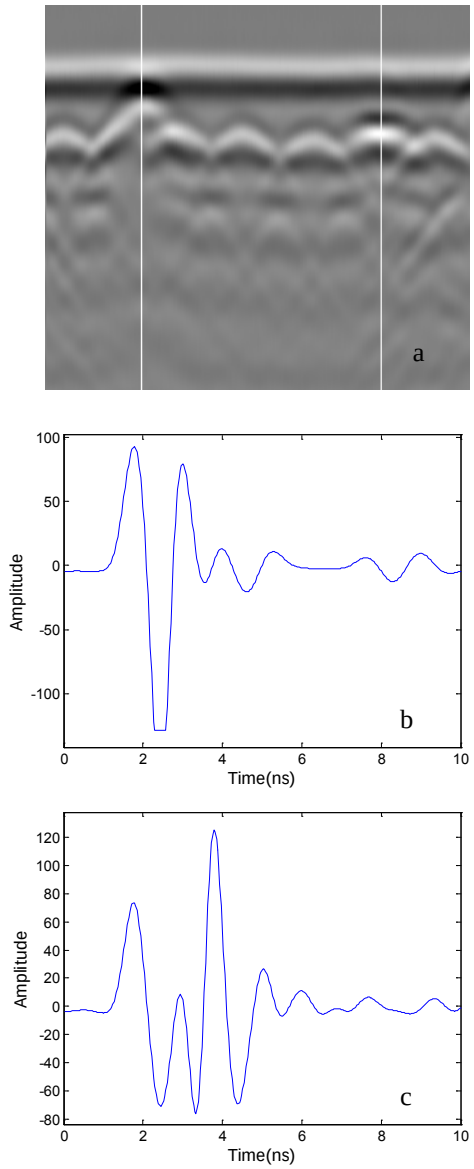

Fig.10: A is a raw GPR scan data from a 6-inch slab with two embedded delamination defects. B and C are extracted traces at columns 75 and 260

The SVD, SSDA, and ICA deconvolution algorithms are used to reduce the overlapping between reflections from closely spaced targets and to estimate the round-trip travel time of GPR waves

to the overlapping targets from which velocity analysis method estimates depth. Table 4 shows actual and estimated depth for the defects of the aforementioned scans. As the table indicates, the average difference between estimated and actual depth is 1.14 cm, 0.91 cm, and 0.53 cm for SVD, SSDA, and ICA algorithms. The SVD, SSDA, and ICA are able to estimate depth within 1.2 cm in 57.1%, 78.6%, and 92.9% of the cases. ICA, under certain circumstances, may give the worst accuracy such as the case of Scan2 with the actual depth of 4.72. This means that ICA gives worst accuracy in one case out of fourteen cases with lowest average difference error among the three deconvolution algorithms, indicating that ICA algorithm has better performance than SVD and SSDA which is in agreement with the results of the synthetic data.

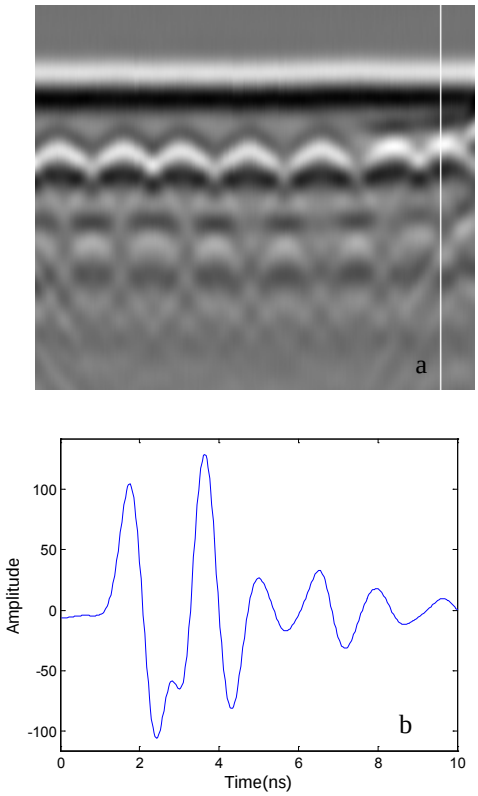

Fig. 11: A is a raw GPR scan data from a 6-inch slab with embedded air-void defect. B is an extracted trace at column 302

Each scan has different acquisition direction, location, and different embedded objects at deferent depths. For example, the first defect of scan 2 masked reflections from underneath objects while the second defect is totally overlapped with rebar reflections. The relative errors of ICA are greater than 40% in only Scan 2 (14.3% of the total scans). The SVD, SSDA, and ICA have relative errors greater than 20% in 85.7%, 71.4%, and 28.6%, respectively. However, the difference error in all cases of ICA is less than 2 cm which is acceptable for bridge deck condition assessment problem.

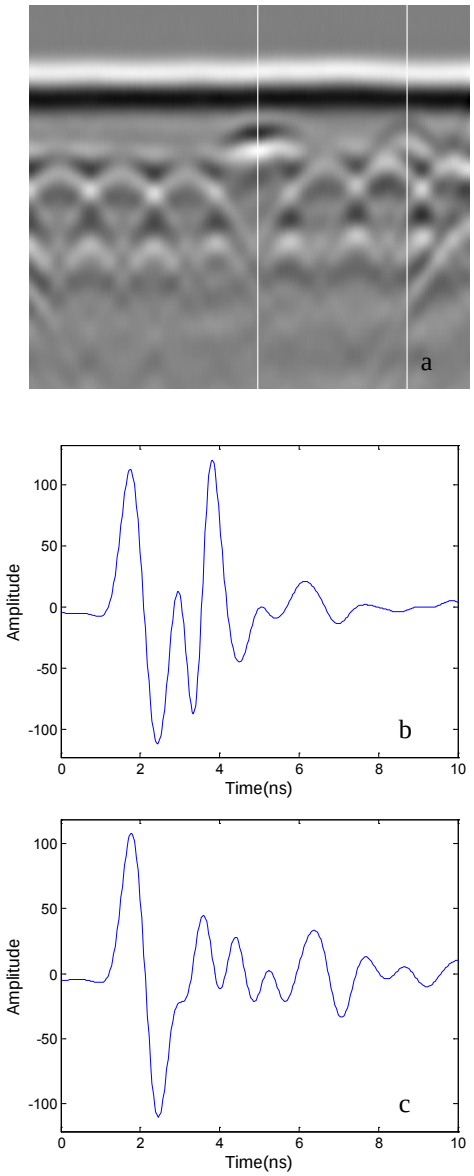

Fig. 12: A is a raw GPR scan data from a 6-inch slab with embedded delamination and air-void defects. B and C are extracted traces at columns 195 and 322

5 Concluding Remarks

Ground Penetrating Radar is a sophisticated nondestructive technique that can be used for detecting internal defects in concrete bridge decks. The underlying motivation behind the work presented in this paper is to automate the process of detecting defects from GPR scans to reduce processing time and increase accuracy of identification for the purposes of bridge condition

assessment, leading to better repair decisions and possibly higher cost savings.

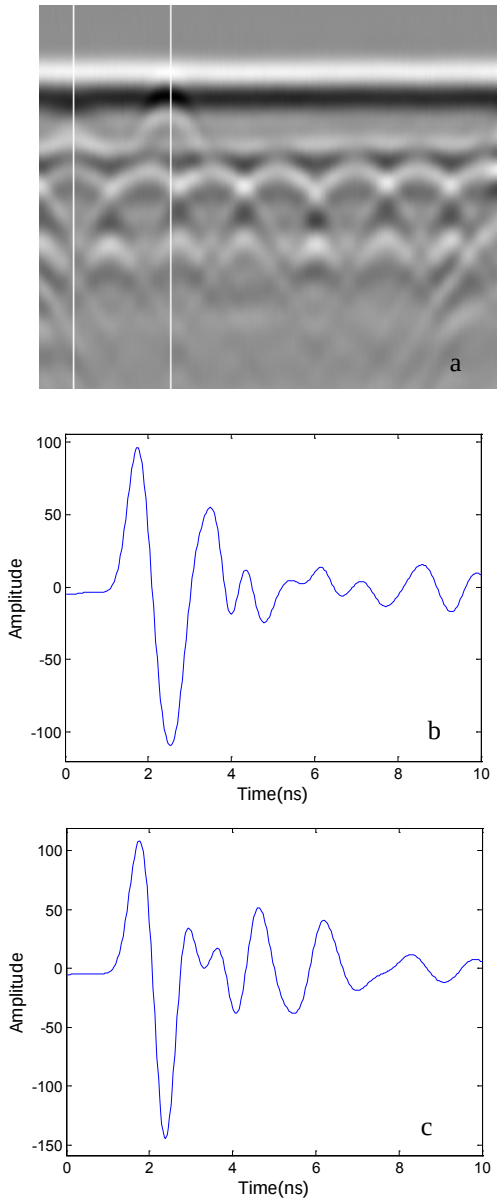

Fig. 13: A is a raw GPR scan data from a 6-inch slab with embedded delamination and air-void defects. B and C are extracted traces at columns 24 and 90

Estimation of the impulse response of concrete bridge decks and their internal objects and defects from raw GPR signals can be modeled as a deconvolution problem. The SVD, SSDA, and ICA algorithms can be used for deconvolution to overcome obstacles such as overlapping between reflections from closely spaced targets. We found that ICA is better than SVD and SSDA in average difference between actual and estimated depth. Also, ICA can estimate depth within 1.2 cm from the actual depth in 92.9% of the cases while SVD in 57.1% and SSDA 78.6%. Finally, SVD and SSDA methods failed to accurately detect spike locations in case of very small differential time delay between the two adjacent spikes.

Two types of GPR scans are used to test the performance of the deconvolution methods. The synthetic data are used to show performance of the deconvolution algorithms in an ideal environment. The experimental data are raw data obtained using the GPR antenna which may contain high and/or low frequency noise. Therefore, the performance of the deconvolution algorithms is compared in the presence of noise.

The ICA algorithm used in this work requires more execution time than SVD and SSDA algorithms which can be improved by utilizing faster ICA methods. All three algorithms in this work are numerical methods used to deconvolute an A-scan without exploiting any prior knowledge of GPR data. Future work should integrate any prior knowledge based on data used and/or defects expected to improve results.

Acknowledgments

Partial support of this work was provided by Western Michigan University FRACAA award. The authors would like to acknowledge Western Michigan University for its support and contributions to the Information Technology and Image Analysis (ITIA) Center.

Table 3: Collected scans from 15-cm slab with different acquisition coordinates

Scan	Defects	Y-axis (cm)	X-axis (cm)
1	Air void	along	100
2	Two delaminations	61	along
3	Air void	94	along
4	Delamination + air void	along	22.9
5	Delamination + air void	along	94
6	Air void	40.6	along
7	Two delaminations	17.8	along
8	Air void	along	104.1
9	Two delaminations	along	78.7

References:

[1] O. Abudayyeh, S. Yehia, I. Abdel-Qader, A. Zalt, GPR imaging for bridge deck condition assessment, *Bridge Structure*, 4(2), 2008, pp. 75-86.

[2] K. Belli, S. Wadia-Fascetti, C. Rappaport, Integrated sensor and media modeling environment developed and applied to ground penetrating radar investigation of bridge decks, *ASCE Journal of Computing in Civil Engineering*, 25(1), 2011, pp. 10-20.

[3] GSSI handbook for radar inspection of concrete, *Geophysical Survey Systems, Inc*. Salem, NH, 2006.

[4] V.A. Lórenz-Fonfría, J. Villaverde, E. Padros, Fourier deconvolution in non-self-deconvolving conditions, Effective narrowing, signal-to-noise degradation, and curve fitting, *Applied Spectroscopy*, 56(2), 2002, pp. 232–242.

[5] C.D. Rennie, R.G. Millar, Deconvolution technique to separate signal from noise in gravel bedload velocity data, *ASCE journal of hydraulic engineering*, 133(8), 2007, pp. 845-856.

[6] A. Lotsch, M. Friedl, J. Pinzon, Spatio–temporal deconvolution of NDVI image sequences using independent component analysis, *IEEE Transactions on geoscience and remote sensing*, 41(12), 2003, pp. 2824-2938.

[7] K. Chahine, V. Baltazart, Y. Wang, X. Derobert, Blind deconvolution via independent component analysis for thin-pavement thickness estimation using GPR, *Non-Destructive Testing in Civil Engineering*, June 30th - July 3rd, 2009.

[8] B. Chen, Z. Geng, T. Shen, Y. Yang, Wavelet-based adaptive regularization deconvolution for turbulence-degraded image, *Proceedings of SPIE-The International Society for Optical Engineering*, 7157 (4), 2009, 71570I (Feb.).

[9] V. Krause, I. Abdel-Qader, Deconvolution and segmentation of ground penetrating radar images, Department of Electrical and Computer Engineering, *Western Michigan University*, Report number 2007-103, 2007.

[10] D. Ghosh, T.K. Sarkar, Extraction of the signature of a buried object using GPR, *IEEE National Radar Conference-Proceedings*, 1631815, 2006, pp. 296-301 (April).

[11] A. Al-Qaisi, W. Woo, S. Dlay, Novel statistical approach to blind recovery of earth signals and source wavelet using independent component analysis, *WSEAS Transactions on Signal Processing*, 4(4), 2008, pp. 231-240.

[12] C.L. Bastard, V. Baltazart, Y. Wang, J. Saillard, Thin pavement thickness estimation using GPR with high and super resolution methods, *IEEE Transactions Geosciences Remote Sensing*, 45(8), 2007, pp. 2511-2519.

[13] E. Rothwell, W. Sun, Time domain deconvolution of transient radar data, *IEEE transactions on antennas and propagation*, 38 (4), 1990, pp. 470-475.

[14] V. Lijn, F. Roth, M. Verhaegen, Estimating the impulse response of buried objects from ground penetrating radar signals, *Proceedings of SPIE-the international society for optical engineering*, 5089 (1), 2003, pp. 387-394.

[15] A. Hyvarinen, J. Karhunen, E. Oja, Independent component analysis, *John Wiley & Sons, Inc*. New York, 2001.

[16] S.T. Kaplan, T.J. Ulrych, Blind deconvolution and ICA with a banded mixing matrix, *4th international symposium on independent component analysis and blind signal separation*, 2003, pp. 591-596 (April).

[17] A. Rudra, Prasanta Chandra Mahalanobis: A biography, *Oxford University Press*, 1996.

[18] Z. Koldovsky, P. Tichavsky, E. Oja, Efficient variant of algorithm FastICA for independent component analysis attaining the cramer-rao lower bound, *IEEE transactions on neural networks*, 17 (5), 2006, pp. 1265-1277.

[19] A. Hyvarinen, Fast and robust fixed-point algorithms for independent component analysis, IEEE transactions on neural networks, 10 (3), 1999, pp. 626-634 (May). engineering, 133(8), 2007, pp. 845-856.

[20] L. Wei, L. Hua-ming, Q. Pei-Wen, Sparsity enhancement for blind deconvolution of ultrasonic signals in nondestructive testing application, *Journal of the optical society of america and review of scientific instruments*, 79, 2008, 014901 (January).

[21] A. Koirala, I. Abdel-Qader, Investigation of deconvolution methods for bridge decks GPR signals, Technical Report 2007-101, *the Information Technology and Image Analysis (ITIA) Center, Western Michigan University*, December, 2007.

Table 4: Actual and estimated defect depth of scans1 through 9

Scan	Actual Depth **(cm)**	Estimated Depth SVD **(cm)**	Diff **(cm)**	Estimated Depth SSDA **(cm)**	Diff **(cm)**	Estimated Depth ICA **(cm)**	Diff **(cm)**
Scan 1	1	1.57	0.57	0.61	0.39	1.09	0.09
Scan 2	2.51	2.92	0.41	4.47	1.96	3.58	1.07
	4.72	3.63	1.09	5.03	0.31	6.71	1.99
Scan 3	3.61	5.31	1.7	4.72	1.11	3.35	0.26
Scan 4	4.72	5.54	0.82	5.08	0.36	4.83	0.11
	3.61	5.99	2.38	4.65	1.04	3.48	0.13
Scan 5	2.51	3.94	1.43	3.71	1.2	1.55	0.96
	1	2.82	1.82	3.66	2.66	0.94	0.06
Scan 6	1	1.53	0.53	1.5	0.5	1.22	0.22
Scan 7	2.92	1.52	1.4	2.28	0.64	2.34	0.58
	4.19	5.83	1.64	2.45	1.74	3.69	0.5
Scan 8	1	1.46	0.46	0.35	0.65	1.26	0.26
Scan 9	4.19	5.33	1.14	4.17	0.02	3.07	1.12
	2.54	1.99	0.55	2.7	0.16	2.44	0.1
Average			**1.14**		**0.91**		**0.53**